Cascarini, F., Hornung, B., Quinn, M. S., Robertson, P., & Orr-Ewing, A. (2019). Collision Energy Dependence of the Competing Mechanisms of Reaction of Chlorine Atoms with Propene. *Journal of Physical Chemistry A*, *123*(13), 2679-2686. https://doi.org/10.1021/acs.jpca.9b01370

Collision Energy Dependence of the Competing Mechanisms of Reaction of Chlorine Atoms with Propene

Frederick J. J. Cascarini, Balázs Hornung, Mitchell S. Quinn, Patrick A. Robertson and Andrew J. Orr-Ewing*

School of Chemistry, University of Bristol, Cantock's Close, Bristol BS8 1TS, United Kingdom

* Author for correspondence. E-mail: a.orr-ewing@bristol.ac.uk

ABSTRACT: Quasi-classical trajectory simulations examine the reaction of Cl with propene across a range of collision energies, from 7 to 28 kJ mol^{-1}. The majority (70% at 7 kJ mol^{-1}, 86% at 14 kJ mol^{-1} and 93% at 28 kJ mol^{-1}) of reactive trajectories produce HCl by direct abstraction of a hydrogen atom from the methyl group of propene, but the remainder involve a variety of delayed mechanisms. Among these longer-lived trajectories, transient formation of an energized 1-chloropropyl radical intermediate is predominant, with only a minor contribution from the 2-chloropropyl radical and roaming pathways. The branching ratios between these intermediate states are largely invariant to collision energy, although the overall proportion of indirect trajectories increases at lower collision energies. The greater role for longer-lived trajectories is reflected in the computed product scattering angle distributions, which become more isotropic at lower energies. However, the distributions of population over vibrational and rotational states of the product HCl do not change with collision energy because they are controlled by the dynamics late along the reaction path.

1. Introduction

The photochemically induced reactions of atomic chlorine with volatile organic compounds (VOCs) in the Earth's atmosphere can start sequences of oxidation reactions similar to the pathways initiated by hydroxyl radical reactions.[1] This chlorine-atom chemistry is particularly significant in the marine boundary layer and in coastal regions.[2-5] Of particular interest are reactions with isoprene and higher terpenes, which constitute 30-50% of biogenic VOCs.[6] Unsaturated organic compounds such as these react with chlorine atoms to produce alkyl or alkenyl radicals, which can react further in the atmosphere to form long-chain enols and enones. These oxygen-containing polar organic compounds contribute to the formation of secondary organic aerosols. However, the mechanisms of reactions of alkenes with chlorine atoms are less studied than those of alkanes, which involve direct hydrogen abstraction pathways to produce alkyl radicals.[7-12] The reactions of Cl atoms with unsaturated VOCs typically exhibit greater mechanistic complexity, with competition between addition and abstraction reactions leading to different outcomes.[13-16] Building on our group's prior experimental and computational studies of the dynamics of prototypical Cl-atom reactions with alkenes,[16-17] the current work explores the factors influencing this competition in the first steps of the Cl-atom initiated chain of atmospheric oxidation reactions of unsaturated VOCs.

Propene is the simplest hydrocarbon to contain both sp^2 (C=C) and sp^3 (-CH_3) hybridized carbon atoms, and its reactions with Cl atoms serve as a simpler analogue to reactions of isoprene and terpenes. The reaction with chlorine atoms under low-pressure conditions ultimately produces HCl and the resonance-stabilized allyl radical (CH_2CHCH_2):

$$Cl + CH_3CHCH_2 \rightarrow HCl + CH_2CHCH_2 \qquad (1)$$

$$\Delta_r H^{\ominus}_{298K} = -63.1 \text{ kJ·mol}^{-1}$$

The presence of the alkene functional group introduces the possibility of reaction pathways other than direct H-atom abstraction. These more complicated mechanisms include formation of a chloropropyl radical adduct,[18-19] which can be stabilized at higher pressure by bath-gas collisions, and "roaming" dynamics, in which the chlorine atom becomes temporarily trapped in the potential well created by the π-orbital of the alkene.[16] Roaming dynamics have previously been well characterised for unimolecular reactions such as the photodissociation of formaldehyde (H_2CO) [20-22] and acetaldehyde.[23-26] Clear-cut evidence is rarer in bimolecular reactions, although roaming contributions have been proposed for reaction of Cl atoms with isobutene, which is expected to be mechanistically similar to (1).[27]

Experimental accounts of the mechanism of reaction (1) demonstrate variations between reactions performed at high collision energies (for example, using translationally

excited Cl atoms from photolysis of a precursor molecule) and at thermal energies. Under the former conditions, velocity map imaging (VMI) experiments suggest direct abstraction dominates,[16] whereas at thermal energies longer-lived intermediates involving addition to the double bond have been argued to increase in significance.[13-14]

We previously reported a global potential energy surface (PES) for reaction (1), obtained as an empirical valence bond (EVB) fit to the *ab initio* computed energies of a range of structures of reactants, intermediates and products. Using this PES, we propagated quasi-classical trajectory (QCT) calculations at collision energies of 28 kJ mol^{-1} to simulate experimental VMI studies.[17] The current work investigates the impact that collision energy has on the reaction mechanism, with the aim of understanding the apparent mechanistic differences observed in the translationally hot and thermal regimes. In particular, we have investigated the relative significance of direct abstraction and addition-elimination mechanisms at a range of collision energies, and have sought supporting evidence for roaming type dynamics.

2. Computational Details

Trajectory simulations were computed using a global EVB PES for reaction (1). This PES, and the methods used to create it, have been described in detail previously;[17] as such, only a brief discussion is included here.

The prior work by Hornung *et al*. developed three EVB-fitted PESs for reaction (1) to unravel the contributions of various features on the multi-dimensional energy landscape to the product scattering and internal energy distributions. Here, we focus on the most complete of these PESs, labelled as EVB3 in reference 17. This EVB surface was fitted to ab-initio points calculated using CCSD(T)-F12B/cc-pVDZ-F12 energies for a wide range of possible structures sampled in all degrees of freedom. The structures were optimised using RMP2/6-311G(d,p) calculations, except for the hydrogen abstraction channel where difficulties in convergence necessitated use of the B3LYP/6-311G(d,p) level of theory. The EVB model was then used to fit the parameters of an EVB matrix, defined in reference 17, to a set of 1000 of these ab-initio points. The outcomes of QCT calculations on this EVB-fitted PES at a collision energy of 28 kJ mol^{-1} were previously compared with experimental data and found to give satisfactory agreement.

Two slices through the global EVB PES of particular significance for the reaction dynamics are depicted in Figure 1. The upper plot shows the locations of the two potential energy wells corresponding to the 1-, and 2-chloropropyl addition complexes (shown in blue/black), as well as the region in which a chlorine atom interacts more loosely with the π-electron system of the alkene (the green area appearing diagonally across the image).

We interfaced the EVB PES with the VENUS program, which was used to propagate classical trajectories over the surface.[28] The starting separation of the centres of mass of the chlorine atom and propene was selected to be 9 Å, with impact parameters randomly sampled at values up to 8 Å, and with random initial orientation of the propene molecule. Reactive trajectories terminated when the HCl product reached a distance of 5 Å from the allyl radical coproduct. All trajectories were propagated with a timestep of 0.150 fs. Batches of trajectories were initiated with initial collision energies in the centre-of-mass frame of either 7 kJ mol^{-1}, 14 kJ mol^{-1} or 28 kJ mol^{-1}. A breakdown of the numbers of trajectories analysed is provided below.

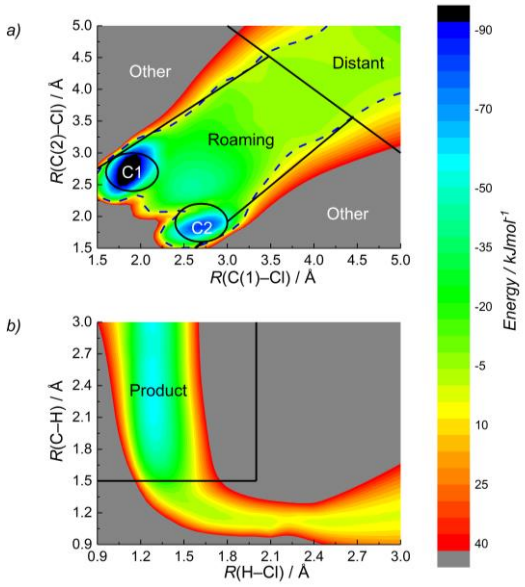

Figure 1: *Depictions of two 2-dimensional slices through the global EVB PES previously reported by Hornung et al.[17] In panel (a), the PES is plotted as a function of the distance of the Cl atom from the terminal and central C-atoms in the C=C bond, C(1) and C(2). In panel (b), the coordinates used are the distance of the Cl from a methyl-group H atom, and the corresponding methyl-C to H distance. The overlaid lines demark areas of the PES used to classify reaction trajectory types, as explained in Table 1. The C1 and C2 labels in (a) identify the 1-chloropropyl and the 2-chloropropyl radical addition complexes, respectively. The dotted line in panel (a) depicts the energy contour at 0 kJ mol^{-1}, which guided our choice of conditions for a roaming assignment.*

The outputs from the trajectory simulations were used to compute distributions of populations of the quantum states of the HCl product, the internal energies of the allyl radical co-product, and scattering angles, as well as opacity functions (describing the probability of reaction at different impact parameters) and reaction times. In addition, selected internal coordinates were recorded every 50th time step, corresponding to a temporal spacing of 7.5 fs.

3. Analysis

Analysis of completed trajectories used custom-written Python and Fortran scripts. The analysis process first considered the internal energy of the products of reaction (1), discarding any trajectories for which the internal energy of either species was below its vibrational zero-point energy. Trajectories that satisfied this check were then classified by whether they ended with a hydrogen atom bonded to the chlorine (reactive trajectories), or with the reactants reforming (unreactive trajectories). The reactive trajectories were further processed by assigning vibrational and rotational quantum states to the HCl using a histogram binning algorithm. Differential cross sections (DCS) were then extracted by fitting the distribution of scattering angles (across all product states) to a sum of Legendre polynomials up to fourth order. Error bars were calculated for the DCS and opacity functions using a bootstrapping process.[29] This process was based on 1000 data sets randomly sampled with replacement from the original data set. The results were used to generate the 95% pointwise confidence interval, which is shown in the corresponding figures. The error bars computed for the vibrational and rotational distributions also represent 95% confidence intervals, based on a margin of error approximated by $N^{-1/2}$.

Table 1. Categories and their Definitions used for Assignment of Trajectories.

Assignment	Definition
Products	R(Cl-H) < 2 Å, R(C(3)-H) > 1.5 Å
Distant	R(C(1)-Cl) + R(C(2)-Cl) > 8 Å
1-chloropropyl radical	$(R(C(1)\text{-}Cl) - 1.9\ Å)^2 + (R(C(2)\text{-}Cl) - 2.7\ Å)^2 \leq 0.09\ Å^2$
2-chloropropyl radical	$(R(C(1)\text{-}Cl) - 2.7\ Å)^2 + (R(C(2)\text{-}Cl) - 1.9\ Å)^2 \leq 0.09\ Å^2$
Roaming region	$1.13 \times R(C(1)\text{-}Cl) - 1.47\ Å \leq R(C(2)\text{-}Cl) \leq 0.89 \times R(C(1)\text{-}Cl) + 1.42\ Å$
Other	a situation that does not satisfy any condition listed above.

Mechanisms of reaction were assigned by analysing the internal coordinates of trajectories at each propagation step using the definitions listed in Table 1. These defined regions classified the reactive trajectories according to the states identified by Hornung *et al.*:[17] the transient formation of energized 1- or 2-chloropropyl radical intermediates; a roaming state; the chlorine atom distant from the propene; and reaction products. The assignment tests were performed in the order they are presented in Table 1, with subsequent criteria only being checked if all prior tests were returned as false.

The definitions listed in Table 1 are based on the identification of different regions of the multi-dimensional EVB PES, as illustrated in Figure 1. In this work, we concentrate in large part on the minority indirect pathways: complex-mediated reactions involve addition to one or other C atom of the double bond to form 1- or 2-chloropropyl radicals transiently before HCl elimination, whereas weaker interactions with the π-electron density of the double bond might result in roaming trajectories across a broad and energetically flat region of the PES. These pathways are not mutually exclusive, because elimination of HCl from an energized chloropropyl radical might involve some degree of roaming dynamics.[27]

The regions corresponding to the two isomers of the chloropropyl radical are visible as deep potential wells in the depiction of the PES in Figure 1(a). Each such assignment is characterized by an elliptical boundary around the appropriate PE well. Assignment of a roaming state is more complicated. In the current work, we assign only an upper limit to the contribution from roaming trajectories by counting those in which the chlorine atom interacts transiently with the π-electron system, with the corresponding weakly attractive region of the PES demarcated in Figure 1(a) and defined numerically in Table 1. The set of trajectory steps identified by this method is a superset of all the trajectories that would satisfy a more precise definition of roaming.[30-31] The quantitative bounds of this assignment were set by linear fits of the coordinates of Figure 1(a) to the 0 kJ mol^{-1} PE contour line of the EVB PES.

4. Results and Discussion

The analysed outcomes for batches of successful quasi-classical trajectories are reported here as populations of HCl quantum states, opacity functions, reaction times, scattering angle distributions, and classifications of reaction mechanisms. The total numbers of computed trajectories that successfully terminated in the allocated computer time, as either reactive or unreactive, were 64695 at a collision energy of 7 kJ mol^{-1}, 134884 at 14 kJ mol^{-1} and 109894 at 28 kJ mol^{-1}. Of these sets of trajectories, 3756, 5848 and 4419 respectively resulted in HCl and allyl radical products. Subsequent checks identified 1772, 2893 and 2252 trajectories at 7, 14 and 28 kJ mol^{-1} collision energies which satisfied our condition of HCl and allyl radical internal energies greater than the zero-point vibrational energies of the two products. Only these final groups of trajectories were retained for further analysis.

4.1 Product HCl Quantum State Populations

Figure 2 depicts the populations of rotational and vibrational levels of the HCl products, at each of the three collision energies studied, normalised by dividing the population in each state by the total population. These population distributions reflect the outcomes of both direct and indirect reaction pathways, and show little or no dependence on the collision energy. This insensitivity to collision energy can be understood if the trajectories sample similar transition state geometries for the H-atom abstraction step in the reaction, regardless of the collision energy and the preceding mechanism to reach the transition state. This result supports the conclusion drawn by Hornung *et al.*[17] using reduced forms of the global EVB PES, that the populations of rotational and vibrational states are controlled by a transition state for

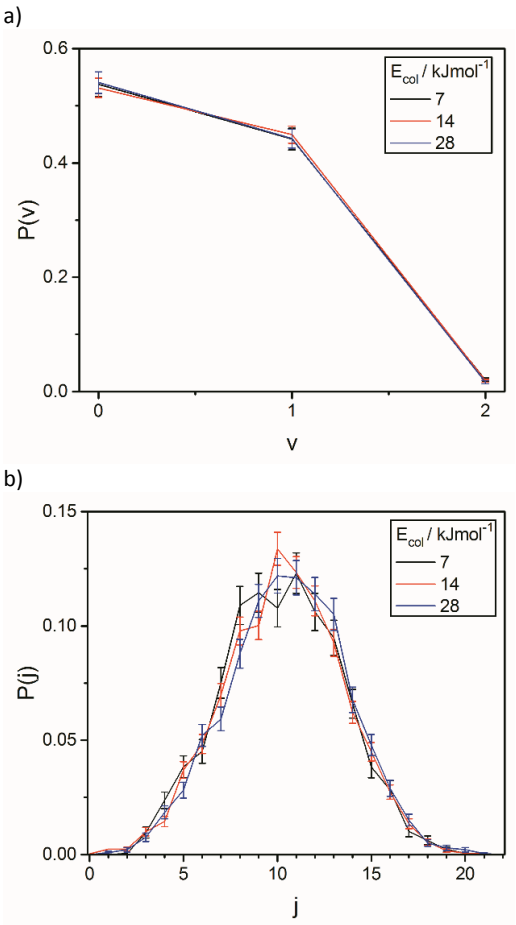

***Figure 2**. Simulated (a) vibrational and (b) rotational level populations of the HCl products of reaction (1) at three different collision energies. The labels v and j denote the vibrational and rotational quantum numbers of the HCl, respectively. The distributions were deduced from the outcomes of classical trajectories propagated on the EVB PES described in the text and illustrated in Figure 1, with initial collision energies of 7 kJ mol^{-1} (black), 14 kJ mol^{-1} (red), or 28 kJ mol^{-1} (blue). They have been normalized such that the sum of all the populations is unity for a given data set.*

H-abstraction which is sampled by both direct and indirect routes, and the shape of the exit valley from the transition state to products. Specifically, the quantum state population distributions computed using a restricted PES allowing only the direct abstraction pathway were the same as those computed using the full EVB PES incorporating 1- and 2-chloropropyl radical complex formation and interactions with the π-electron cloud of the C=C bond. The current work extends the conclusions from the prior study by demonstrating that, even with the full topography of the global EVB PES available for dynamical exploration, the collision energy of the reaction has negligible impact on the final HCl product quantum state population distribution. Below, we show that the collision energy does impact on the proportion of long-lived intermediates sampled by the trajectories, but these competitive indirect and direct pathways to reach the H-abstraction transition state do not ultimately influence the product state population distributions.

4.2 Impact Parameter and Reaction Time

Opacity functions plotted in Figure 3 depict the dependence of reaction probability on the initial impact parameter. They are normalized such that the corresponding distributions expressed in terms of the reduced impact parameter (equation 2) integrate to unity.[32]

$$b_{red} = \frac{2b^2}{b_{max}^2} - 1 \qquad (2)$$

The plots show enhanced reactivity at higher impact parameters for lower collision energies, which is consistent with long-range attractive and barrierless interactions drawing the reactants together more effectively when the collision energy is smaller.

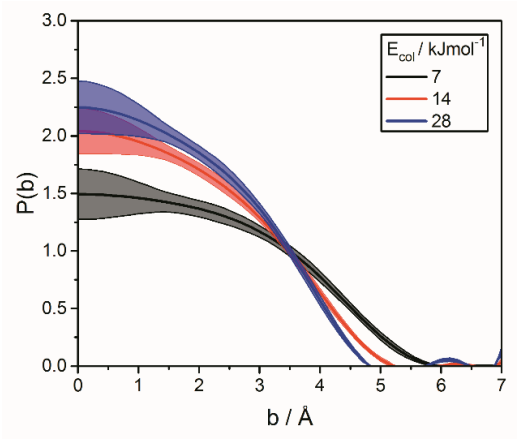

***Figure 3.** Dependence of reaction probability on the initial impact parameter, b. Computed opacity functions, P(b) are shown for the three collision energies studied, with the inset key defining the colour scheme used. Solid lines are the computed*

distributions, with the shaded surrounding areas showing uncertainties at the 95% confidence level.

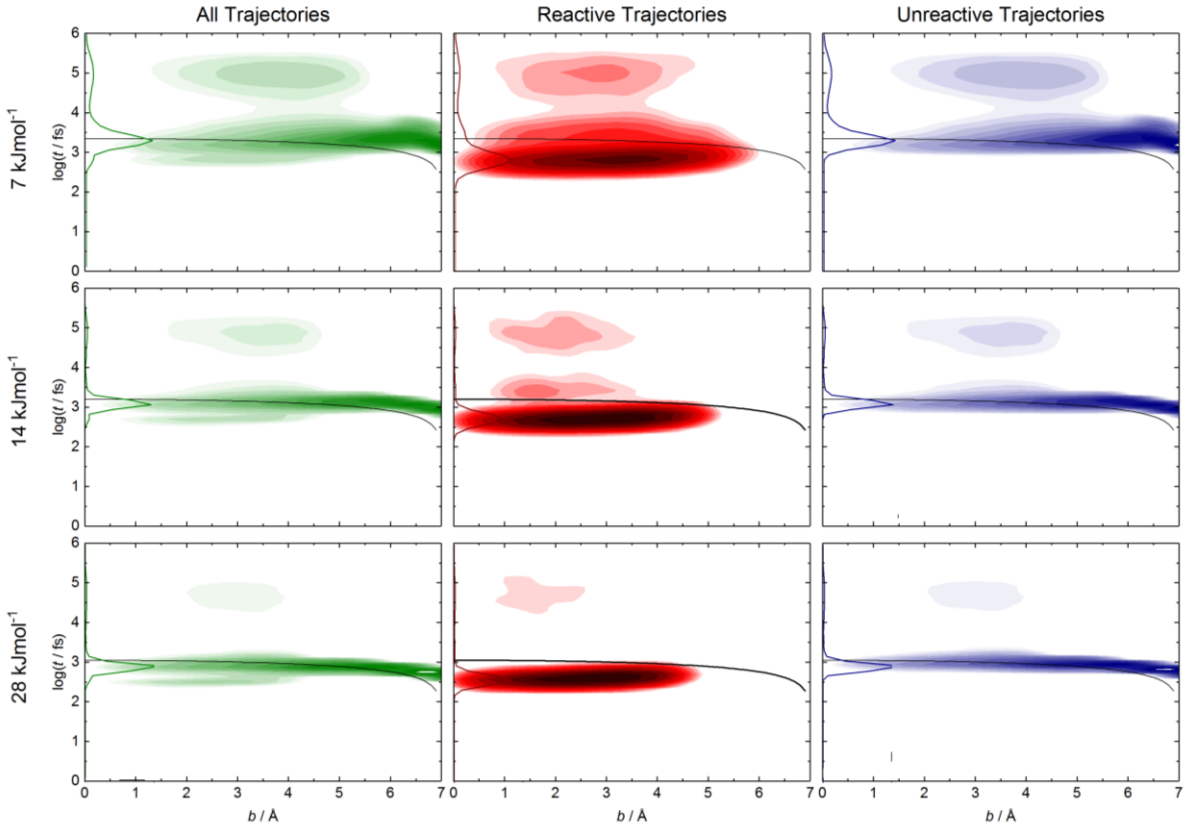

Figure 4. *Depictions of the dependence of trajectory durations (plotted as the base-10 logarithms of trajectory completion times) on initial impact parameter, for the three collision energies studied. The three columns classify the trajectories as unreactive (right), reactive (centre) and the sum of reactive and unreactive outcomes (left). Trajectory outcomes are shown by colour maps, which use a base-10 logarithmic scaling to highlight the long-lived features, and are compared to the timescale for bypass of a propene molecule by a Cl atom with the same starting collision energy and a range of impact parameters (black solid lines). The functions plotted alongside the ordinates depict kernel density estimations of the trajectory outcomes as a function of time, in arbitrary units.*

The plots in Figure 4 explore this behaviour further by displaying how the computed trends in reaction time depend on impact parameter for our three different choices of collision energies. The behaviour for reactive and unreactive trajectories is also compared. The plots reveal some of the consequences of changing collision energy on the reaction dynamics and mechanisms.

It is useful to compare the trajectory time distributions for unreactive trajectories to those expected for simple bypassing trajectories in which the chlorine passes the propene molecule without any intermolecular interactions. The dependence of this bypass time on impact parameter is depicted by the black lines plotted in the panels in Figure 4. This timescale is reduced at high impact parameters because of the spherical initialization and termination conditions of the trajectory simulation, which are defined for the chlorine being a certain radius from the centre of the propene molecule. As such, the distance between the initialization and termination locations in the event of no interaction between the two species reduces at higher impact parameters, because the distance across a sphere centred at the propene centre of mass decreases.

Unreactive trajectories closely follow the model bypass trajectory timings, especially at higher collision energies, with only the lowest collision energy dataset showing any significant deviation. In contrast, reactive trajectories frequently exhibit timings faster than would be expected of a bypass trajectory. This behaviour is attributed to acceleration caused by attractive interactions between the Cl atom and the propene molecule during the direct abstraction trajectories which dominate the reactivity. Moreover, apportioning some of the exothermicity of reaction to product translation can increase the kinetic energy of the products compared to reactants.

At the higher collision energies of 14 and 28 kJ mol^{-1}, trajectory completion times close to the bypass timescale dominate for both reactive and unreactive data sets. For reactive collisions, 93% (28 kJ mol^{-1} collision energy) and 86% (14 kJ mol^{-1} collision energy) of these trajectories are

best characterized as direct abstraction of a hydrogen atom from the methyl group of propene. At the 7 kJ mol^{-1} collision energy, 70% of reactive trajectories are direct, and a secondary peak in the distribution of reaction times becomes more prominent at longer delays. This alternative scattering behaviour is evidence of long-lived intermediates. Its presence in the analysis of both reactive and unreactive trajectories demonstrates that the participation of these long-lived states does not preclude either dissociation back into the reactants or progression on to the reactive transition state. The likely cause is a contribution from energized 1- or 2-chloropropyl addition complexes, and perhaps also roaming dynamics. These possibilities are explored further in section 4.4.

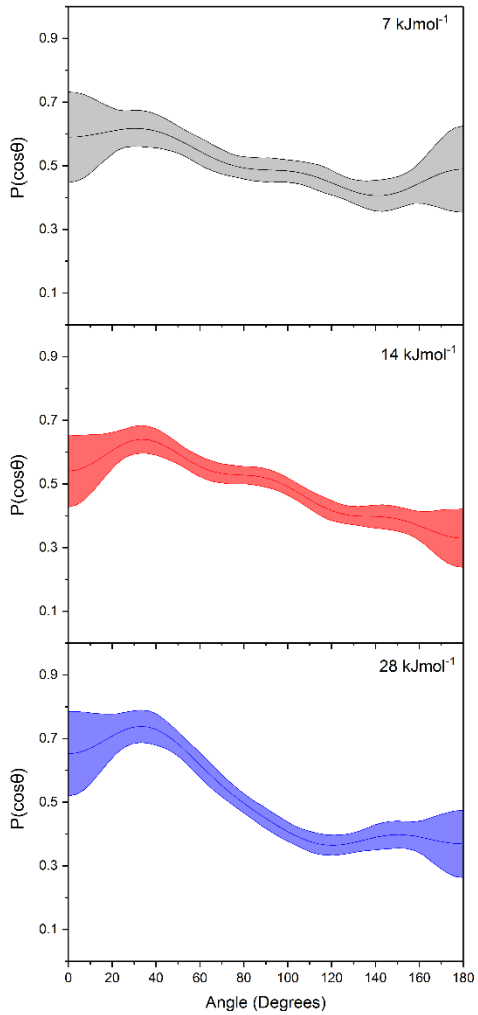

Figure 5. *Computed distributions (solid lines) of product HCl scattering angles, defined with respect to the relative velocity of the Cl-atom. The distributions are shown for 3 collision energies; 7 kJ mol^{-1} (top, black), 14 kJ mol^{-1} (middle, red) and 28 kJ mol^{-1} (bottom, blue), and are summed over all product HCl vibrational and rotational quantum states. The distributions are calculated as a normalised fit of the cosine of the scattering angle to a sum of Legendre polynomials. The order of the Legendre expansion has been selected independently at each energy through a minimisation of the statistical risk. The shaded areas depict the 95% confidence interval of the mean.*

4.3 Scattering Angle Distributions

Fitted distributions of HCl scattering angles, summed over all vibrational and rotational quantum states, are plotted in Figure 5 for the three collision energies. At the higher collision energies, most products are forward scattered, although a broad distribution is characteristic of facile abstraction of an H-atom from an sp^3-hybridized carbon atom.[8, 11-12, 27, 33-35] However, the scattering angle distributions becomes increasingly isotropic at lower collision energies, supporting the findings reported in Section 4.2 of the growing importance of long-lived intermediates, and possible steering of Cl-atom approach directions by long-range attractive forces. The plots in Figure 4 indicate that these complexes survive for timescales of 10^4 – 10^5 fs, which exceed the rotational period of the energized chloropropyl radicals.

4.4 Trajectory Assignments

As was noted in Section 4.2, most of the reactive trajectories at the three collision energies considered involve direct abstraction of an H-atom. Here, we focus on the minority of indirect trajectories, which show more complicated reaction dynamics. The contribution to reaction by indirect pathways involving long-lived addition complexes is confirmed by further examination of the stepwise progression of the reactive trajectories. We performed this analysis on a set of 1308 trajectories at 7 kJ mol^{-1}, 2535 at 14 kJ mol^{-1} and 4527 at 28 kJ mol^{-1}. After the first few picoseconds of product build-up, which are dominated by direct abstraction reactions, quantitative analysis of the remaining incomplete trajectories shows that the 1-chloropropyl radical is strongly favoured: more than 80% of the delayed trajectories exist as this intermediate at any single timestep. This preference is shown in Figure 6, which displays the proportions of trajectories assigned to the categories listed in Table 1 at each timestep.

Focussing on the indirect trajectories after direct reactions have completed, Figure 6 shows that the relative proportion of each assignment type remains largely invariant over time. Although the long-lived trajectories become more important as a proportion of all reactive trajectories at lower collision energies (reactive trajectories lasting longer than 1.5 ps increase from 7% at 28 kJ mol^{-1} to 30% at 7 kJ mol^{-1}), the balance of types of these long-lived trajectories does not change.

There is a clear preference for formation of the 1-chloropropyl radical intermediate over the 2-chloropropyl radical at all collision energies. This observation agrees with experimental measurements by Lee and Rowland, who reported measured branching ratios of 1-chloropropyl to 2-chloropropyl radicals that varied from 6.6 ± 0.1 to 12.3 ± 0.1, depending on the

partial pressures of the reactants.[18] To compare with these experimental values, we calculated the ratio of the total time spent by all reactive trajectories as these two different isomers of the chloropropyl radical. This analysis yields 1-chloropropyl to 2-chloropropyl radical ratios of 16 at 28 kJ mol^{-1} and 11 at 7 kJ mol^{-1}. At 14 kJ mol^{-1}, a larger number of trajectories were propagated, giving a total of 17897 reactive trajectories, to test the consistency of these ratios. A bootstrapping analysis of these trajectory outcomes using 1000 samples produced a mean ratio of 23 ± 7 at the 95% confidence interval. If we apply this uncertainty in the ratio to the 7 kJ mol^{-1} calculations, the computed values overlap the experimental ratios reported by Lee and Rowland. The calculations indicate that the 1-chloropropyl radical is consistently favoured over the 2-chloropropyl radical for the range of collision energies studied.

A more complete analysis of the trajectories which continue beyond 1 ps, before forming HCl + allyl radical products, provides the classification ratios reported in Table 2. These values demonstrate that the 1 chloropropyl structure is sampled for more than three quarters of the duration of these indirect reactive trajectories. Notwithstanding the lenient definition of roaming structures in this study, we find only around a tenth of the total time of propagation of the indirect trajectories is spent in a roaming assignment.

Further analysis shows that a significant amount of these roaming assignments involved fast (few fs) excursions from the 1-chloropropyl assignment. This behaviour suggests excess internal energy in the 1-chloropropyl radical occasionally localizes sufficiently in a C-Cl bond to induce large-amplitude vibrational motion. To study this effect further, 211 long-lived (> 1.5 ps) reactive trajectories at a collision energy of 7 kJ mol^{-1} were randomly selected. The assignments of these trajectories were then modified such that any set of roaming assignments in adjacent 7.5-fs time bins that did not span at least 10 time bins (i.e., 75 fs), was changed to the assignment immediately following the set. The basis for this reassignment was that roaming dynamics are mechanistically distinct from single oscillations of large-amplitude vibrational motions extending beyond the PES regions defined as 1- or 2-chloropropyl in our analysis (Table 1). This procedure reduced the roaming assignment proportion to 2.5% of the total time.

***Table 2**: Proportions of Time Spent by Indirect Reactive Trajectories in Each Assignment.*

Trajectory type	Percentage of time		
	7 kJ mol^{-1}	*14 kJ mol^{-1}*	*28 kJ mol^{-1}*
1-chloropropyl	78.2%	81.6%	80.1%
2-chloropropyl	7.0%	2.5%	4.9%
Roaming[(a)]	10.2%	10.8%	11.5%
Distant	4.1%	4.6%	2.9%
Products	0.2%	0.2%	0.2%
Other	0.3%	0.3%	0.4%

[(a)] See main text for further discussion

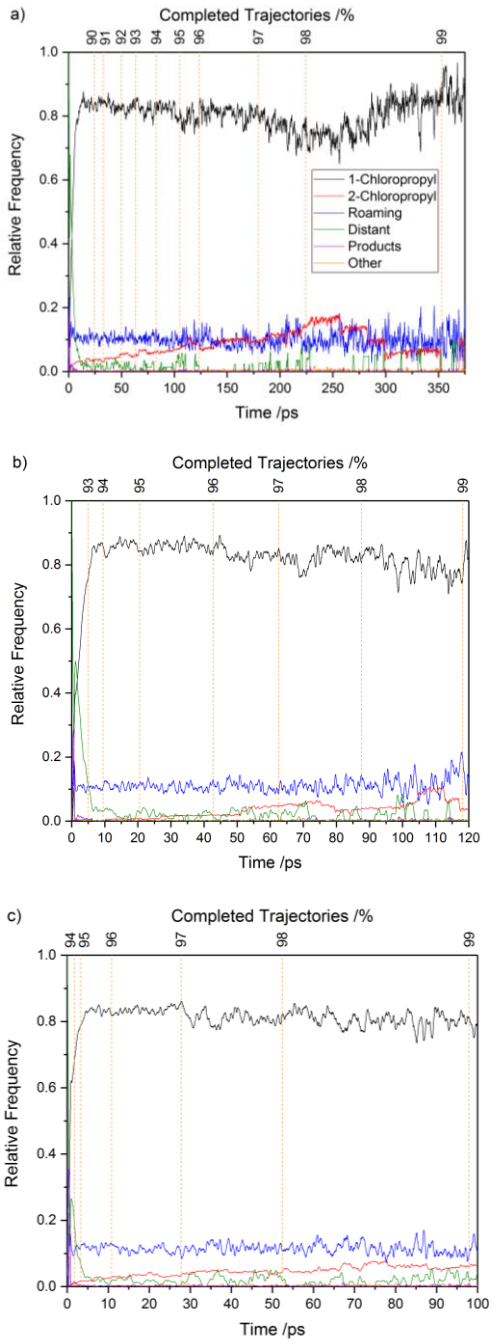

***Figure 6**. The proportion of incomplete reactive trajectories assigned to intermediates corresponding to different regions of the PES at each timestep. The inset keys provide the colour codes for the different intermediates. The plots show the outcomes for ensembles of trajectories propagated at initial collision energies of: (a) 7 kJ mol^{-1}; (b) 14 kJ mol^{-1}; and (c) 28 kJ mol^{-1}. The top axis in each plot depicts the percentages of trajectories that have completed at given timesteps. The data were smoothed using a second-order Savitzky-Golay filter with a 0.9975-ps width. The graphs are curtailed shortly beyond 99% completion of trajectories.*

5. Conclusions

The exothermic reaction of Cl atoms with propene to make HCl serves as a benchmark system to understand the dynamics of Cl-atom reactions with unsaturated hydrocarbons. Quasi-classical trajectory calculations using a full-dimensionality PES developed previously by Hornung *et al*., are used to explore the collision energy dependence of the reaction dynamics. Direct abstraction of an H-atom from the terminal methyl group of the propene, with reaction complete within 1 ps, is the dominant pathway at the three collision energies studied (7, 14 and 28 kJ mol^{-1}) but the minor contribution of indirect pathways increases as the collision energy decreases. The regions of the global PES sampled by these indirect pathways are classified as energized 1-chloropropyl radical and 2-chloropropyl radical adducts, or roaming-encounter and distant-encounter complexes (the latter arguably corresponding to long-range roaming dynamics). At all three collision energies studied, the indirect trajectories spend approximately 80% of their time sampling the 1-chloropropyl radical PE well, and less than 10% in the vicinity of the 2-chloropropyl PE well. The trajectories sampled the roaming potential energy region for ~10% of their time. However, significant amounts of this time arise from high frequency motion across our chosen boundary between the 1-chloropropyl radical state and the roaming region. When we reclassify these motions as large-amplitude vibrations of the energized chloropropyl radicals, the roaming proportion reduces dramatically. The calculations demonstrate that distributions of product HCl populations among vibrational and rotational levels are insensitive to the initial collision energy, but that the range of impact parameters leading to successful reaction widens at lower collision energies. This effect, and the small increase in propensity for indirect dynamics, cause more isotropic scattering of the products in the centre-of-mass frame as the collision energy decreases. The results go some way to bridge the gap between molecular beam studies of the dynamics of the Cl + propene reaction at elevated collision energies and the studies of reaction rate coefficients, product HCl vibrational excitation, and trapping of 1- and 2-chloropropyl radical intermediates performed under thermalized conditions. The QCT analysis provides new insights for the likely mechanisms of reactions of Cl atoms with various unsaturated VOCs of natural and anthropogenic origins in the troposphere.

Acknowledgments

This work was support by EPSRC Programme Grant EP/L005913/1. FJJC thanks the EPSRC for award of Doctoral Training Grant funding (EP/N509619/1).

References

1. Walavalkar, M.; Sharma, A.; Alwe, H. D.; Pushpa, K. K.; Dhanya, S.; Naik, P. D.; Bajaj, P. N., Cl Atom Initiated Oxidation of 1-Alkenes under Atmospheric Conditions. *Atmos. Environ.* **2013,** *67*, 93-100.

2. Singh, H. B.; Gregory, G. L.; Anderson, B.; Browell, E.; Sachse, G. W.; Davis, D. D.; Crawford, J.; Bradshaw, J. D.; Talbot, R.; Blake, D. R.*, et al.*, Low Ozone in the Marine Boundary Layer of the Tropical Pacific Ocean: Photochemical Loss, Chlorine Atoms, and Entrainment. *J. Geophys. Res., D: Atmos.* **1996,** *101*, 1907-1917.

3. Spicer, C. W.; Chapman, E. G.; Finlayson-Pitts, B. J.; Plastridge, R. A.; Hubbe, J. M.; Fast, J. D.; Berkowitz, C. M., Unexpectedly High Concentrations of Molecular Chlorine in Coastal Air. *Nature* **1998,** *394*, 353-356.

4. Tanaka, P. L.; Oldfield, S.; Neece, J. D.; Mullins, C. B.; Allen, D. T., Anthropogenic Sources of Chlorine and Ozone Formation in Urban Atmospheres. *Environ. Sci. Technol.* **2000,** *34*, 4470-4473.

5. Thornton, J. A.; Kercher, J. P.; Riedel, T. P.; Wagner, N. L.; Cozic, J.; Holloway, J. S.; Dube, W. P.; Wolfe, G. M.; Quinn, P. K.; Middlebrook, A. M.*, et al.*, A Large Atomic Chlorine Source Inferred from Mid-Continental Reactive Nitrogen Chemistry. *Nature* **2010,** *464*, 271-274.

6. Arneth, A.; Schurgers, G.; Lathiere, J.; Duhl, T.; Beerling, D. J.; Hewitt, C. N.; Martin, M.; Guenther, A., Global Terrestrial Isoprene Emission Models: Sensitivity to Variability in Climate and Vegetation. *Atmos. Chem. Phys.* **2011,** *11*, 8037-8052.

7. Murray, C.; Orr-Ewing, A. J., The Dynamics of Chlorine-Atom Reactions with Polyatomic Organic Molecules. *Int. Rev. Phys. Chem.* **2004,** *23*, 435-482.

8. Hornung, B.; Harvey, J. N.; Preston, T. J.; Dunning, G. T.; Orr-Ewing, A. J., Empirical Valence Bond Theory Studies of the $CH_4 + Cl \rightarrow CH_3 + HCl$ Reaction. *J. Phys. Chem. A* **2015,** *119*, 9590-9598.

9. Pilgrim, J. S.; McIlroy, A.; Taatjes, C. A., Kinetics of Cl Atom Reactions with Methane, Ethane, and Propane from 292 to 800 K. *J. Phys. Chem. A* **1997,** *101*, 1873-1880.

10. Bottoni, A.; Poggi, G., An Ab-Initio Study of Hydrogen Abstraction by Fluorine, Chlorine and Bromine Atoms from Ethane and Propane. *J. Mol. Struct.: THEOCHEM* **1995,** *337*, 161-172.

11. Estillore, A. D.; Visger-Kiefer, L. M.; Ghani, T. A.; Suits, A. G., Dynamics of H and D Abstraction in the Reaction of Cl Atom with Butane-1,1,1,4,4,4-D_6. *Phys. Chem. Chem. Phys.* **2011,** *13*, 8433-8440.

12. Pandit, S.; Hornung, B.; Dunning, G. T.; Preston, T. J.; Brazener, K.; Orr-Ewing, A. J., Primary vs. Secondary H-Atom Abstraction in the Cl-Atom Reaction with n-Pentane. *Phys. Chem. Chem. Phys.* **2017,** *19*, 1614-1626.

13. Pilgrim, J. S.; Taatjes, C. A., Infrared Absorption Probing of the Cl + C_3H_6 reaction: Rate Coefficients for Hcl Production between 290 and 800 K. *J. Phys. Chem. A* **1997,** *101*, 5776-5782.

14. Coquet, S.; Ariya, P. A., Kinetics of the Gas-Phase Reactions of Cl Atom with Selected C2-C5 Unsaturated Hydrocarbons at 283 < T < 323 K. *Int. J. Chem. Kinet.* **2000,** *32*, 478-484.

15. Kaiser, E. W.; Wallington, T. J., Temperature (290–400 K) and Pressure (5–900 Torr) Dependence of the Kinetics of the Reactions of Chlorine Atoms with

Propene and 1-Butene. *Chem. Phys. Lett.* **2011,** *501*, 187-192.
16. Preston, T. J.; Dunning, G. T.; Orr-Ewing, A. J.; Vazquez, S. A., Direct and Indirect Hydrogen Abstraction in Cl + Alkene Reactions. *J. Phys. Chem. A* **2014,** *118*, 5595-5607.
17. Hornung, B.; Preston, T. J.; Pandit, S.; Harvey, J. N.; Orr-Ewing, A. J., Computational Study of Competition between Direct Abstraction and Addition-Elimination in the Reaction of Cl Atoms with Propene. *J. Phys. Chem. A* **2015,** *119*, 9452-9464.
18. Lee, F. S. C.; Rowland, F. S., Thermal Chlorine-38 Reactions with Propene. *J. Phys. Chem.* **1977,** *81*, 1222-1229.
19. Kaiser, E. W.; Wallington, T. J., Pressure Dependence of the Reaction Cl+C_3H_6. *J. Phys. Chem.* **1996,** *100*, 9788-9793.
20. Bowman, J. M., Skirting the Transition State, a New Paradigm in Reaction Rate Theory. *Proc. Natl. Acad. Sci. U. S. A.* **2006,** *103*, 16061-16062.
21. Suits, A. G., Roaming Atoms and Radicals: A New Mechanism in Molecular Dissociation. *Acc. Chem. Res.* **2008,** *41*, 873-881.
22. Quinn, M. S.; Andrews, D. U.; Nauta, K.; Jordan, M. J. T.; Kable, S. H., The Energy Dependence of CO(v,j) Produced from H_2CO Via the Transition State, Roaming, and Triple Fragmentation Channels. *J. Chem. Phys.* **2017,** *147*, 013935.
23. Heazlewood, B. R.; Jordan, M. J.; Kable, S. H.; Selby, T. M.; Osborn, D. L.; Shepler, B. C.; Braams, B. J.; Bowman, J. M., Roaming Is the Dominant Mechanism for Molecular Products in Acetaldehyde Photodissociation. *Proc. Natl. Acad. Sci. U. S. A.* **2008,** *105*, 12719-12724.
24. Sivaramakrishnan, R.; Michael, J. V.; Klippenstein, S. J., Direct Observation of Roaming Radicals in the Thermal Decomposition of Acetaldehyde. *J. Phys. Chem. A* **2010,** *114*, 755-764.
25. Shepler, B. C.; Braams, B. J.; Bowman, J. M., Quasiclassical Trajectory Calculations of Acetaldehyde Dissociation on a Global Potential Energy Surface Indicate Significant Non-Transition State Dynamics. *J. Phys. Chem. A* **2007,** *111*, 8282-8285.
26. Rubio-Lago, L.; Amaral, G. A.; Arregui, A.; Izquierdo, J. G.; Wang, F.; Zaouris, D.; Kitsopoulos, T. N.; Banares, L., Slice Imaging of the Photodissociation of Acetaldehyde at 248 nm. Evidence of a Roaming Mechanism. *Phys. Chem. Chem. Phys.* **2007,** *9*, 6123-6127.
27. Joalland, B.; Shi, Y.; Kamasah, A.; Suits, A. G.; Mebel, A. M., Roaming Dynamics in Radical Addition-Elimination Reactions. *Nat Commun* **2014,** *5*, 4064.
28. Hase, W. L.; Duchovic, R. J.; Hu, X.; Komornicki, A.; Lim, K. F.; Lu, D.-H.; Peslherbe, G. H.; Swamy, K.; Vande Linde, S. R.; Varandas, A.*, et al.*, Venus96: A General Chemical Dynamics Computer Program. *QCPE Bull.* **1996,** *16*, 671.
29. Efron, B.; Tibshirani, R.; Tibshirani, R. J., *An Introduction to the Bootstrap*. Chapman & Hall: New York, 1993.
30. Houston, P. L.; Conte, R.; Bowman, J. M., Roaming under the Microscope: Trajectory Study of Formaldehyde Dissociation. *J. Phys. Chem. A* **2016,** *120*, 5103-5114.
31. Cofer-Shabica, D. V.; Stratt, R. M., What Is Special About How Roaming Chemical Reactions Traverse Their Potential Surfaces? Differences in Geodesic Paths between Roaming and Non-Roaming Events. *J. Chem. Phys.* **2017,** *146*, 214303.
32. Aoiz, F. J.; Herrero, V. J.; Sáez Rábanos, V., Quasiclassical State to State Reaction Cross Sections for D+H_2(v=0, j=0)→HD(v',j')+H. Formation and Characteristics of Short-Lived Collision Complexes. *J. Chem. Phys.* **1992,** *97*, 7423-7436.
33. Abou-Chahine, F.; Greaves, S. J.; Dunning, G. T.; Orr-Ewing, A. J.; Greetham, G. M.; Clark, I. P.; Towrie, M., Vibrationally Resolved Dynamics of the Reaction of Cl Atoms with 2,3-Dimethylbut-2-ene in Chlorinated Solvents. *Chem. Sci.* **2013,** *4*, 226-237.
34. Estillore, A. D.; Visger, L. M.; Suits, A. G., Crossed-Beam DC Slice Imaging of Chlorine Atom Reactions with Pentane Isomers. *J. Chem. Phys.* **2010,** *132*, 164313.
35. Huang, C.; Li, W.; Suits, A. G., Rotationally Resolved Reactive Scattering: Imaging Detailed Cl+C_2H_6 Reaction Dynamics. *J. Chem. Phys.* **2006,** *125*, 133107.

TOC Graphic

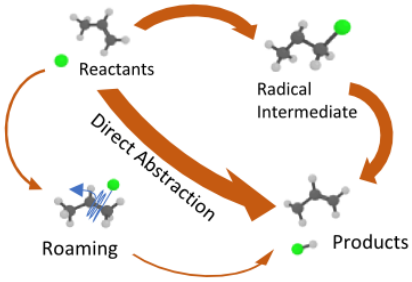
Reactants
Radical
Intermediate
Direct Abstraction
Roaming
Products